Applied Acoustics 202 (2023) 109150

Contents lists available at ScienceDirect

Applied Acoustics

journal homepage: www.elsevier.com/locate/apacoust

Dual parameters optimization l_p-LMS for estimating underwater acoustic channel with uncertain sparsity

Zhengliang Zhu [a,b], Feng Tong [a,b,*], Yuehai Zhou [a,b], Feiyun Wu [c]

[a] College of Ocean and Earth Sciences, Xiamen University, Xiamen, China
[b] National and Local Joint Engineering Research Center for Navigation and Location Service Technology, Xiamen University, Xiamen, China
[c] School of Marine Science and Technology, Northwestern Polytechnical University, Xi'an, China

ARTICLE INFO

Article history:
Received 28 July 2022
Received in revised form 13 October 2022
Accepted 25 November 2022

Keywords:
Least mean square (LMS)
p-norm-like constraint
Dual parameters optimization
Underwater acoustic communication

ABSTRACT

The sparse norm constraint (l_0, l_1, l_2 and l_p) least mean square algorithm (LMS) is established technique for modeling sparse systems. However, when applied in target systems with uncertain sparsity, such as temporal-spatial-varying sparse underwater acoustic (UWA) channel, the parameters tuning (the step-size and parameter p) of l_p-LMS faces significant challenges. In this paper, with the purpose to simplify the complicated dual-parameter selection problem via gradient strategy, a dual parameters optimization l_p-LMS (DPO-l_p-LMS) algorithm is derived by iteratively adjusting the step-size and the parameters p in parallel along the descent gradient. Convergence analysis of the proposed algorithm is given. A numerical simulation under varying sparsity systems exhibits that the proposed algorithm outperforms the l_p-LMS algorithms driven by the existing optimization approaches in convergence speed and steady-state error. Meanwhile, a field shallow water experiment of UWA communication demonstrated that the proposed algorithm achieves superior performance under the framework of direct adaptation turbo equalization (DA-TEQ).

1. Introduction

The adaptive filter algorithms have been widely utilized in various applications such as beamforming, channel estimation, and channel equalization, within which the least mean square (LMS) algorithm developed by Windrow and Hoff [1] features its simplicity, robustness, and low computational complexity. In practical, sparse system [2] that only contains a tiny proportion of significant coefficients in the whole impulse response widely exists in popular scenarios such as wireless communication channels and underwater acoustic (UWA) channels. Because the standard LMS does not consider this type of sparse prior information, sparsity exploitation under the framework of the LMS algorithm draws significant attention from the sparse system research community.

To enhance the modelling accuracy as well as to improve the convergence performance of the adaptive filter for sparse systems, some sparsity-exploitation LMS algorithms have been developed in recent years [3–13]. The general solution for sparsity exploitation adaptive filter algorithm can be classified into two categories, 1) proportionate-based adaptive algorithm, 2) sparse norm constraint-based adaptive algorithm. In the proportionate-based adaptive algorithm, different step-size is allocated to each filter coefficient depend on the magnitude of the corresponding filter weight coefficients named proportionate normalized LMS (PNLMS) [12]. Althought the PNLMS offer good convergence behavior in sparse system, but the performance is impacted in case of non-sparse system. An improved PNLMS was reported in [13] that improve the performance in case of sparse and non-sparse scenarios. In the sparse norm constraint-based adaptive algorithm, several sparse norm constraints have been incorporated into the cost function of the standard LMS. In [3–5], Gu Yuantao et.al. proposed l_0-LMS, l_1-LMS by incorborating the l_0, l_1 norm into the classical LMS for enhancing the convergence speed of zero coefficients. For l_0-LMS, l_1-LMS, the convergence analysis are given in [7,8]. The essence of these works lies in imposing various zero attraction (ZA) factors on zero and non-zero coefficients of the weights. Similar ideas are also used in normalized-LMS (NLMS), non-uniform norm constraint LMS (NNCLMS) [3,4,6]. Recently, A modified Versoria function-based ZA-LMS (MVZA-LMS), joint logarithmic hyperbolic cosine adaptive filter (JLHCAF) algorithm was developed in [10,11], which achieve faster convergence speed and better modelling accuracy.

Returning to the definition of the norm, it is a metric of matrix or vector. From this view, l_0, l_1 norm constrain lack of sparse adaptation factor, which indicates that the performance of l_0, l_1-LMS

* Corresponding author.

https://doi.org/10.1016/j.apacoust.2022.109150
0003-682X/

will be impacted when the sparsity of the unknown system changes. Thus, the p-norm-like constrain enable well aware the sparsity of unknown system compare with the l_0 and l_1 norm via adjusting the parameter p [14,15]. In [16], a gradient optimization p-norm-like constraint LMS (called l_p-LMS) was proposed, with the parameter p adjusting with the sparsity of the system. The numerical simulations show that the l_p-LMS performs better than l_0, l_1-LMS. However, the l_p-lms discussed in [16] only use a constant step-size. Thus it can not achieve a fast convergence rate and lower mean square error (MSE) simultaneously.

For l_p-lms, many step-size optimization approaches such as variable step-size (VSS) mechanism [17,18] have been done via using a quantity linear/nonlinear function, which constructs the relation between the instantaneous error and step-size [19–21]. In [22], the VSS-l_p-LMS was proposed by Wang et al., the modified Gaussian function was used to adjust the step-size, and the VSS function was constructed by the moving average method. Similar investigations have been reported in [23,24]. Note that, herein this type of l_p-LMS algorithms driven by signle parameter optimization is called simple parameters optimization l_p-LMS (SPO-l_p-LMS) algorithm.

However, for target systems with uncertain sparsity, such as the UWA channel, sparsity patterns experience temporal-spatial variations due to complicated propagation mechanisms and diverse reflections at static or dynamic boundaries. To be specific, the sparse pattern of the UWA channel consists of two parts, one is the relatively stationary or slowly changing arrival multipaths caused by the direct path or the bottom reflection [25]. The other is the rapidly time-varying arrivals which is mainly caused by the random unevenness of the ocean interface, the non-uniformity of the seawater medium, and the multipath caused by the organisms, air bubbles, wind waves and internal waves in the ocean [26,27]. From the physical mechanism of sound propagation, the latter one presents time-varying and uncertain. Thus, the overall underwater acoustic channel presents a time-varying dynamical property with uncertain sparsity. Some field experiments of underwater acoustic channels in [28–32] verify the property of uncertainty sparsity, and the research in [33,34] reveals that explicitly exploiting the uncertainty sparsity of UWA channels can achieve better communication performance. As p parameter and step-size parameter is designed to offer adjustability for sparsity pattern and convergence-misadjustments, respectively, in such a target system with uncertain sparsity, tuning the parameters of l_p-LMS faces significant challenges. By simplifying the optimization of p and step-size parameter into a gradient descent problem, we try to develop a dual parameters optimization l_p-LMS (DPO-l_p-LMS) algorithm to seek a tradeoff between algorithm performance and computational complexity in the presence of uncertain sparsity.

The novel contributions of this paper are as follows. First, a dual parameters optimization l_p-LMS (DPO-l_p-LMS) algorithm for temporal-spatial varying sparse UWA channel is derived by adopting gradient descent search for iteratively updating parameter p and step-size in parallel. The bound of the step-size function is derived, ensuring the convergence of the proposed algorithm. Second, we compare the algorithm performance under the different VSS mechanisms based on the framework of l_p-LMS. The numerical simulations show that the proposed DPO-l_p-LMS performs better than l_p-LMS aided by other VSS mechanisms.

The rest part of this paper proceeds as follows. In Section 2, the principle of sparse norm constrain LMS algorithms are briefly described, and the principle of the VSS is explained. The proposed DPO-l_p-LMS algorithm derivation and its convergence analysis are illustrated in Section 3. Section 4, Section 5 presents numerical simulation and experimental results analysis, demonstrating the performance comparison among the l_p-LMS with different VSS mechanisms and LMS. Section 6 concludes this article.

Notation: The vectors are represented by lowercase letters, $(\cdot)^*, (\cdot)^H$, and $(\cdot)^T$ represents the conjugate operator, the conjugate transpose operator, and the transpose operator, respectively. $|\cdot|$ represents the absolute value, $E(\cdot)$ represents the expectation operator, $tr[\cdot]$ denotes as a trace operator, and $\Re(\cdot)$ represents the real part operator.

2. Brief review of sparse norm constraint LMS with variable step-size mechanism

The block diagram of a typical system/inverse system identification problem is shown in Fig. 1 [1]. In this figure, considering the input vector of the adaptive filter is $\mathbf{x}(n) = [x(n), x(n-1), \cdots, x(n-L+1)]^T$, $\mathbf{w}(n) = [w_0(n), w_1(n), \cdots, w_{L-1}(n)]^T$ is the filter weights, $\mathbf{v}(n)$ is the background/system noise, the L and n represents the filter length and the discrete time instant, respectively. Thus, the estimated error between the adaptive filter output and expected output $d(n)$ at nth iterative computation, i.e.

$$e(n) = d(n) - \mathbf{x}^T(n)\mathbf{w}(n). \tag{1}$$

For the sparse norm constraint LMS (l_0-LMS, l_1-LMS, l_p-LMS), the cost function is as follows:

$$J_{sp-lms} = \frac{1}{2}|e(n)|^2 + \gamma||\mathbf{w}(n)||_p, \tag{2}$$

where $0 < \gamma < 1$ is a balanced factor. The constraint item $||\mathbf{w}(n)||_p$ can be stated as follows for different sparse norm constraint LMS algorithm:

$$||\mathbf{w}(n)||_p = \begin{cases} |\mathrm{supp}(\mathbf{w})| & ,p = 0 \\ \sum_{i=1}^{L}|w_i(n)|^1 & ,p = 1 \\ \sum_{u=1}^{L}|w_i(n)|^p & ,0 < p < 1 \end{cases}, \tag{3}$$

where the supp$(\cdot)$ means the position set of the non-zero elements, the L is the filter length. Specially, when $0 \leqslant p \leq 1$, the $||\cdot||_p$ be termed as p-norm-like.

The convergence speed and steady-state error are the primary indicators of LMS performance. The pursuit of increasing the convergence rate or reducing the steady-state error is the motivation for developing improved norm constraint LMS. Many studies on VSS mechanisms have been done to promote the convergence rate of the adaptive algorithm. Some typical VSS mechanisms are summarized in Table 1. The essence of the VSS mechanism is using the step-size sequence instead of the constant step-size.

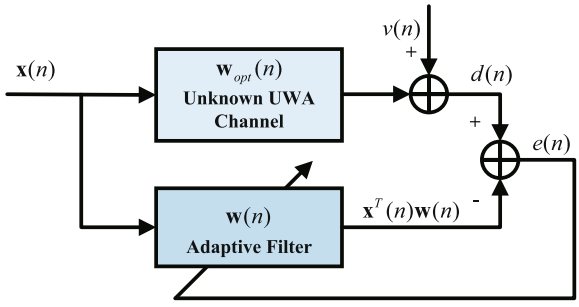

Fig. 1. Block diagram of a typical system/inverse system identification problem.

Table 1
The summary of VSS mechanisms.

Step-size update equation	Parameters	References	Denotation	Computational Complexity
$\mu = \beta\mu(n-1) + (1-\beta)a\|e(n)\|^2 exp(-b\|e(n)\|^2)$	a, b, β	[22]	VSS1	$\mathbf{O}(n)$
$\mu = \beta\{\frac{1}{1+exp(-\alpha\|e(n)\|^m)} - 0.5\}$	α, β, m	[19]	VSS2	$\mathbf{O}(n)$
$\mu = \beta \tanh(\alpha\|e(n)\|^\gamma)$	α, β, γ	[20]	VSS3	$\mathbf{O}(n)$
$\mu = c\{1 - exp(-a\|e(n)\|^b)\}$	a, b, c	[21]	VSS4	$\mathbf{O}(n)$
$\mu = \alpha\mu(n-1) + \gamma e^2(n-1)$	α, γ	[23,24]	VSS5	$\mathbf{O}(n)$
$\mu = \alpha\mu(n-1) + \gamma\theta(n-1)$ $\theta(n-1) = \frac{a}{b}\theta(n-2) + \frac{e^2(n-1)e^2(n-2)}{B(n-1)}$ $B(n) = \sum_{j=0}^{n-1} b^j e^2(n-j-1)e^2(n-j-2)$	α, γ, a, b	[23]	MRVSS	$\mathbf{O}(n^2)$
$\mu = \mu(n-1) + \alpha\frac{\partial J\{e^2(n)\}}{\partial\mu}$	α	[35,36]	DPO	$\mathbf{O}(n)$

Collectively, the implementation ideas of the variable step-size mechanisms can be categorized as follows under two different criteria:

1) utilize the instantaneous error to map the step-size function via linear/non-linear function

$$\mu(n) = \mathbf{f}(\mu(n-1), e(n)), \tag{4}$$

where $\mathbf{f}(\cdot)$ denotes the step-size mapping function.

2) use the optimization approach to achieve the optimal step-size

$$\mu_{opt} = \text{argmin}||J_{sp-lms}||. \tag{5}$$

Dirctly addressing the Eq. (5) to obtain optimum step-size is a complicated optimization problem. In spired by the gradient optimization for the parameter p [16], a novel stragety of simultaneously optimizting step-size and p at each iteration, call dual parameters optimization l_p LMS (DPO-l_p-LMS), is illustrated in the Section 3. Note that, for the purpose of comparison, we incorporate the VSS mechanism mentioned in Table 1 with l_p-LMS and named them follows: VSS1-l_p-LMS, VSS2-l_p-LMS, VSS3-l_p-LMS, VSS4-l_p-LMS, VSS5-l_p-LMS, and MRVSS-l_p-LMS.

3. Derivation and discussion of the proposed algorithm

This section presents the derivation of the proposed algorithm, the convergence analysis, and a brief discussion of the effect of the algorithm parameters.

3.1. Derivation of the proposed DPO-l_p-LMS

Generally speaking, simultaneously optimizing the parameter p and the step-size is a complicated multi-parameter optimization problem involving the highly non-linear supersurface. Herein a novel DPO-l_p-LMS algorithm is derived by simplifying it into a parallel gradient descent iteration [16,35] from the perspective of approximate simplification. Specially, for the l_p-LMS, the corresponding cost function can be expressed as follow [16]:

$$\begin{aligned} &J_p = \tfrac{1}{2}|e(n)|^2 + \gamma||\mathbf{w}(n)||_p \\ &||\mathbf{w}(n)||_p = \sum_{i=1}^{L}|w_i(n)|^p, 0 < p < 1. \end{aligned} \tag{6}$$

The updated equation of the step-size μ can be obtained:

$$\mu(n) \quad = \mu(n-1) + \alpha\Re(\tfrac{\partial J_p}{\partial\mu})(n), \tag{7}$$

where the $\frac{\partial J_p}{\partial\mu}$ can be derived from the Eq. (6), namely:

$$\begin{aligned} &\tfrac{\partial J_p}{\partial\mu} = e(n)\mathbf{x}^H(n)\mathbf{g}^*(n-1) + \\ &\gamma p \cdot \text{sgn}[|\mathbf{w}(n-1)|] \cdot [\mathbf{w}(n-1)]\mathbf{g}(n-1), \end{aligned} \tag{8}$$

where $\mathbf{g}(n) = \frac{\partial\mathbf{w}(n)}{\partial\mu}$, $\beta = \gamma p$.

Using the update equation of l_p-LMS, the iterative equation of $\mathbf{g}$ can be written as follow:

$$\begin{aligned} &\mathbf{g}(n) = \mathbf{g}(n-1) + \mathbf{x}(n)e^*(n) - \mu\mathbf{x}^*(n)\mathbf{x}^T(n)\mathbf{g}(n-1) \\ &-\gamma p(p-1) \cdot \text{sgn}[|\mathbf{w}(n)|]^2 \cdot |\mathbf{w}(n)|^{p-2} \cdot \mathbf{g}(n-1). \end{aligned} \tag{9}$$

The gradient of the cost function (2), (3) with respect to the p can be written as:

$$\begin{aligned} G_p(n) \quad &= \tfrac{\partial\left(\frac{1}{2}|e(n)|^2 + \gamma|\mathbf{w}(n)|^p\right)}{\partial p} \\ &= \gamma|\mathbf{w}(n)|^p \ln(|\mathbf{w}(n)|). \end{aligned} \tag{10}$$

Following the numerical analysis in [16], the sign function of $G_p(n)$ is uesed to reduce the possibility at local minimums,

$$\text{sgn}(G_p(n)) = \text{sgn}(|\mathbf{w}(n)| - \mathbf{I}), \tag{11}$$

where $\mathbf{I}$ is a unit column vector with the same size of $\mathbf{w}(n)$. Thus, the optimization formulation of p can be simplified by as follow:

$$\begin{aligned} p_{n+T} \quad &= p_n - \delta\text{sgn}[\tfrac{1}{T}\sum_{j=n}^{n+T} G_p(j)] \\ &= p_n - \delta\text{sgn}[\tfrac{1}{T}\sum_{j=n}^{n+T}|w_j(n)| - 1], \end{aligned} \tag{12}$$

where the δ is the step-size for controlling the descent gradient updating, and the T is the update periods of p. For avoiding p overflow and leading to norm constrain failure, the newest p is limited between 0 and 1. Namely,

$$p_{n+T} = \begin{cases} \min(p_{n+T}, 0.99), p_{n+T} \geqslant 1 \\ \max(p_{n+T}, 0.01), p_{n+T} \leq 0 \end{cases}. \tag{13}$$

Consequently, the proposed algorithm is described using MATLAB like pseudo-codes, as illustrated in **Algorithm 1**.

Algorithm 1: Pseudo-codes of the proposed algorithm (DPO-l_p-LMS)

Given : $\mu_{ini}, \kappa, p, \epsilon, \alpha, \beta, \delta, L, T$
Initial : $\mathbf{w} = zeros(L, 1), \mu(1) = \mu_{ini}$
For n = 1, 2, $\cdots$, do
Input new $\mathbf{x}(n)$ and $d(n)$;
$e(n) = d(n) - \mathbf{x}(n)^T\mathbf{w}(n)$;
The optimization of parameter p**:**
$p_{n+T} = p_n - \delta\text{sgn}(\frac{1}{T}\sum_n^{n+T}|\mathbf{w}(n)| - 1)$

(*continued on next page*)

(*continued*)

Algorithm 1: Pseudo-codes of the proposed algorithm (DPO-l_p-LMS)

The optimization of step-size:

7: optimize the step-size $\mu(n)$ based on Eqs. (7)–(9)

8: $\mathbf{w}(n+1) = \mathbf{w}(n) + \mu(n)e(n)\mathbf{x}^*(n) - \kappa\frac{p_{n+T}\mathrm{sgn}|\mathbf{w}(n)|}{\epsilon+|\mathbf{w}(n)|^{1-p_{n+T}}}$

Output: filter weights $\mathbf{w}$

3.2. Brief discussion

The section will provide a brief convergence analysis of the proposed algorithm.

Define the filter weight error vectors as:

$$\mathbf{v}(n) = \mathbf{w}(n) - \mathbf{w}_o, \tag{14}$$

where the $\mathbf{w}_o$ is the expected output vector.

Here, four assumptions are assumed for analysis: 1) the input sequence $\mathbf{x}(n)$ is the Gaussian sequence with zero mean and the variance is $\mathbf{R}_\mathbf{x}$; 2) the input sequence $\mathbf{x}(n)$ independent of $\mathbf{w}(n)$; 3) $e(n) \sim N(0, \delta_e^2)$ and independent of $\mathbf{x}(n), \mathbf{w}(n)$, respectively; 4) the step-size $\mu(n)$ also is independent of $\mathbf{x}(n), \mathbf{w}(n)$, respectively.

Correspondingly, based on the **Algorithm 1**, we can obtain:

$$\begin{aligned}&\mathbf{v}(n+1) = (\mathbf{I} - \mu(n)\mathbf{x}(n)\mathbf{x}^T(n))\mathbf{v}(n)\\&+\mu(n)\mathbf{x}(n)e^*(n) - \gamma\frac{p\mathrm{sgn}|\mathbf{w}(n)|}{|\mathbf{w}(n)|^{1-p}}\\&= (\mathbf{I} - \mu(n)\mathbf{R})\mathbf{v}(n) + \mu(n)\mathbf{x}(n)e^*(n) - \mathbf{B},\end{aligned} \tag{15}$$

where: $\mathbf{R} = \mathbf{x}(n)\mathbf{x}^T(n), \mathbf{B} = \gamma\frac{p\mathrm{sgn}|\mathbf{w}(n)|}{|\mathbf{w}(n)|^{1-p}}$.

The covariance matrix of $\mathbf{g}(n+1)$ can be expressed as follow:

$$\begin{aligned}&E[\mathbf{v}(n+1)\mathbf{v}^T(n+1)] = E[\mathbf{v}(n)\mathbf{v}^T(n)]\\&-\mu(n)E[\mathbf{v}(n)\mathbf{v}^T(n)\mathbf{x}(n)\mathbf{x}^T(n)] - E[\mathbf{v}(n)\mathbf{B}^T]\\&-\mu(n)E[\mathbf{x}(n)\mathbf{x}^T(n)\mathbf{v}(n)\mathbf{v}^T(n)]\\&+\mu^2(n)E[\mathbf{x}(n)\mathbf{x}^T(n)\mathbf{v}(n)\mathbf{v}^T(n)\mathbf{x}(n)\mathbf{x}^T(n)]\\&+\mu(n)E[\mathbf{x}(n)\mathbf{x}^T(n)\mathbf{g}(n)\mathbf{B}^T]\\&+\mu^2(n)E[e^*(n)e^*(n)\mathbf{x}(n)\mathbf{x}^T(n)] - E[\mathbf{B}\mathbf{g}^T(n)]\\&+\mu(n)E[\mathbf{B}\mathbf{v}^T(n)\mathbf{x}(n)\mathbf{x}^T(n)] + E[\mathbf{B}\mathbf{B}^T],\end{aligned} \tag{16}$$

To simplify the expression of Eq. (16), denote $\mathbf{S}(n+1) = E[\mathbf{v}(n+1)\mathbf{g}^T(n+1)], \mathbf{S}(n) = E[\mathbf{v}(n)\mathbf{v}^T(n)]$, and $E[\mathbf{x}(n)\mathbf{x}^T(n)] = \mathbf{R}_\mathbf{x}$, the Eq. (16) can be written as [37]:

$$\begin{aligned}&\mathbf{S}(n+1) = \mathbf{S}(n) - \mu(n)\mathbf{S}(n)\mathbf{R}_\mathbf{x}\\&-E[\mathbf{v}(n)\mathbf{B}^T] - \mu(n)\mathbf{R}_\mathbf{x}\mathbf{S}(n)\\&+2\mu^2(n)[\mathbf{R}_\mathbf{x}\mathbf{S}(n)\mathbf{R}_\mathbf{x}]\\&+\mu^2(n)\mathbf{R}_\mathbf{x}\mathrm{tr}(\mathbf{R}_\mathbf{x}\mathbf{S}(n))\\&+\mu(n)\mathbf{R}_\mathbf{x}E[\mathbf{v}(n)\mathbf{B}^T] + \mu^2(n)\delta_e^2\mathbf{R}_\mathbf{x}\\&-E[\mathbf{B}\mathbf{v}^T(n)] + \mu(n)E[\mathbf{B}\mathbf{v}^T(n)]\mathbf{R}_\mathbf{x} + E[\mathbf{B}\mathbf{B}^T].\end{aligned} \tag{17}$$

The trace operator is imposed on the (17), we obtain:

$$\begin{aligned}&tr[\mathbf{S}(n+1)] \leqslant \mu(n)tr[\mathbf{R}_\mathbf{x}E[\mathbf{v}(n)\mathbf{B}^T]] - tr[E[\mathbf{B}\mathbf{v}^T(n)]]\\&+\mu^2(n)\delta_e^2tr[\mathbf{R}_\mathbf{x}] - tr[E[\mathbf{v}(n)\mathbf{B}^T] + tr[E[\mathbf{B}\mathbf{B}^T]]\\&+\mu(n)tr[E[\mathbf{B}\mathbf{v}^T(n)]\mathbf{R}_\mathbf{x}] + tr[\mathbf{S}(n)]\times\\&\{1 - 2\mu(n)tr[\mathbf{R}_\mathbf{x}] + \mu^2(n)tr^2[\mathbf{R}_\mathbf{x}] + 2\mu^2(n)tr[\mathbf{R}_\mathbf{x}^2]\},\end{aligned} \tag{18}$$

where the $E[\mathbf{v}(n)\mathbf{B}^T], E[\mathbf{B}\mathbf{B}^T]$ is bounded [16]. Therefore, the convergence of the euqation (18) depend on:

$$|1 - 2\mu(n)tr[\mathbf{R}_\mathbf{x}] + \mu^2(n)tr^2[\mathbf{R}_\mathbf{x}] + 2\mu^2(n)tr[\mathbf{R}_\mathbf{x}^2]| < 1. \tag{19}$$

Thus, if the $\mu(n)$ meets the Eq. (19), the proposed algorithm will convergence:

$$0 < \mu(n) < \frac{2tr[\mathbf{R}_\mathbf{x}]}{tr^2[\mathbf{R}_\mathbf{x}] + 2tr[\mathbf{R}_\mathbf{x}^2]}. \tag{20}$$

The parameters of proposed the algorithm can be selected as follows:

The choice of κ, p, δ: the initialization of these parameters, can be referenced from [16].

The choice of $\alpha, \beta, \mathbf{g}$: the function of these parameters is adapted to adjust the step size in each iteration. In DPO-l_p-LMS, the parameter α must be set as a small positive value that helps avoid algorithmic divergence. It should be noted that a small positive value does not mean a small positive α will enable a high modeling accuracy. For the parameter β, its selection has a wide adjustment range, $\beta \in (0, 1)$, which affects the step-size. For $\mathbf{g}$, the initial value must be set $\mathbf{g} = 0$.

The computational complexity: The computational complexity per iteration of the standard l_p-LMS algorithms is listed in [16]. For the proposed algorithm, compared with standard l_p-LMS algorithms, the computational complexity increases mainly because of the VSS mechanism, which is given in Table 1.

4. Numerical simulation

In this Section, the proposed DPO-l_p-LMS is compared with LMS, l_p-LMS driven by other VSS mechanisms (summarized in Table 1) in the application of UWA channel estimation via numerical simulations. The UWA channels are generated by the Bellhop ray-tracing software [38], the simulation settings are provided in Table 2, and the corresponding simulation channels are depicted in the Fig. 2. It can be seen from Fig. 2 that the simulation channels at different receiving depths show spatial varying sparsity patterns, corresponding to different sparsity ratio (SR) which is defined as the ratio of non-zero tap counts (with an amplitude large than 0.1) to the total channel length [6].

The transmitted signal in all experiments is a Gaussian sequence with zero mean and unit variance. The corresponding signal-to-noise ratio (SNR) is 15 dB. All results are obtained from 100 times Monte Carlo simulation. The mean square deviation (MSD) is used to evaluate the performances of all compared algorithms:

$$MSD = E[||\mathbf{h}_{est} - \mathbf{h}_\mathbf{0}||_2^2], \tag{21}$$

where $\mathbf{h}_{est}$ is the estimated channel from different algorithms, $\mathbf{h}_\mathbf{0}$ denotes the ground-truth of the channel.

The first experiment investigates the performance of DPO-l_p-LMS with varied parameters α, β, and the simulation channel (Sim-Ch1) are adopted in this experiment.

The second experiment is designed to test the convergence performance of the proposed algorithm under various SRs. The simulation channels (Sim-Ch2, Sim-Ch3, and Sim-Ch4) are employed in this experiment. The SR of the unknown system changes twice

Table 2
Simlation parameters used in Bellhop Model

Simulation Parameters	Value
Carriers frequency [kHz]	15.5
The depth of water [m]	8
Transmitter depth [m]	4
Receiver depth [m]	1, 3, 5, 7
Communication distance [km]	1
Sound source angle [°]	[−60, 60]
Sound speed [m/s]	1511.00

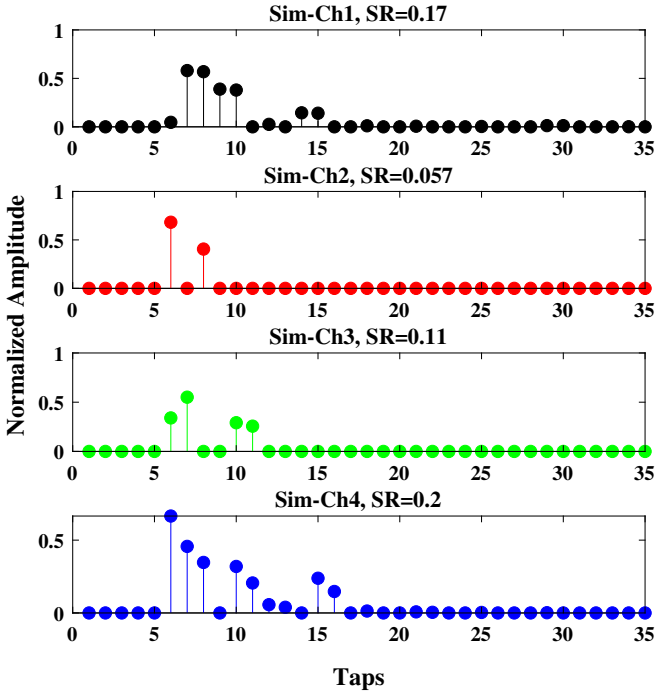

Fig. 2. Simulation channels at different receiving depths. (Sim-Ch1, Sim-Ch2, Sim-Ch3 and Sim-Ch4 correspond to the receivers at different depths, 1 m, 3 m, 5 m, and 7 m, respectively.).

throughout this simulation, at 5000th and 10000th, corresponding to 0.057, and 0.2.

Fig. 3 and Fig. 4 reveal the algorithm performance under various parameter settings. Except for $\alpha \in [9e-8, 9e-7, 2e-6, 9e-6]$, other parameters are fixed: $\mu_{ini} = 5e-3, \kappa = 3e-4$, $\beta = 4e-2, \mathbf{g} = 0$. Fig. 3 shows the MSD curves of proposed algorithms with different α. It can be seen from Fig. 3 that too small α will impact the performance of the proposed algorithm. Furthermore, the large α will accelerate convergence and reduce the MSD. Contrary to the set up pararmeters mentioned previous, the parameter fixed except β, namely, $\mu_{ini} = 5e-3$, $\kappa = 3e-4, \alpha = 2e-6, \mathbf{g} = 0, \beta \in [1e-3, 5e-2, 5e-1]$. The performances with different β driven by Sim-Ch1 are shown in Fig. 4. It can be referred to that the various β have little impact

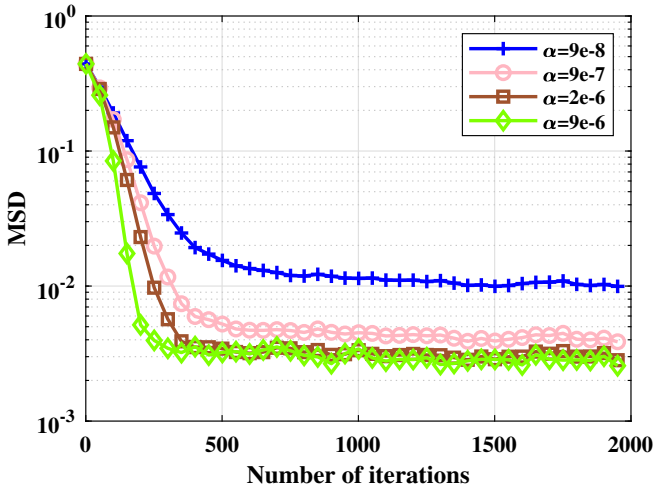

Fig. 3. MSD curves of DPO-l_p-LMS with different α driven by Sim-Ch1.

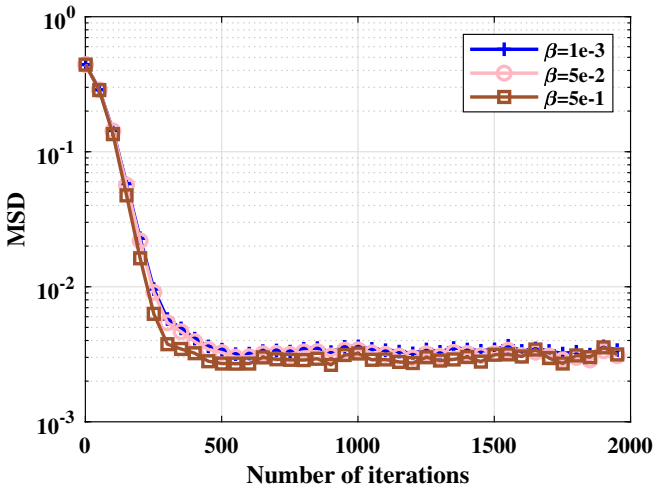

Fig. 4. MSD curves of DPO-l_p-LMS with different β driven by Sim-Ch1.

on the performance, and the hefty β enables to obtain a higher convergence speed for the proposed algorithm.

The simulation results of the second experiment driven by Sim-Ch2, Sim-Ch3, and Sim-Ch3 are presented in Fig. 5 and Fig. 6. The MSD curves of the proposed algorithm and other algorithms (LMS, MVZA-LMS, JLHCAF) are given in Fig. 5. The parameters of candidate algorithms are carefully chosen to make their convergence speed the same and provided in Table 3. At the initial 5000 iterations, namely the system stays in most sparse (SR = 0.057), DPO-l_p-LMS, MVZA-LMS, and JLHCAF obtains a low steady-state MSD than LMS. As the sparsity of the system changes, i.e., the SR changes from 0.057 to 0.2, the MVZA-LMS algorithm shows a significant performance degradation and is worse than LMS. The LMS and the JLHCAF algorithm are more robust in the sparsity-change system, the reason is that the LMS algorithm does not have a sparse constraint item, while the JLHCAF algorithm has. Although the JLHCAF has a sparse aware item, its sparse aware constraint term plays a weak role in the case of same step-size parameters. The DPO-l_p-LMS algorithm obtains a large performance gain compared with the LMS algorithm in the more sparse system because of the optimization of the step-size and the parameter p. When the SR increased, the gap in convergence MSD between the proposed algorithm and the LMS algorithm narrows, which means that in a less sparse system, the performance of the proposed algorithm will be impacted and tend towards the LMS algorithm.

Fig. 6 compares proposed DPO-l_p-LMS with the l_p-LMS aided by different VSS mechanisms. It is worth noting that the algorithms denoted by the legend in Fig. 6 are consistent with Table 1. The parameters of all compared algorithms are carefully chosen as given in Table 4 to optimize the minimum steady-state MSD of each algorithm for the initial 5000 iterations. Various VSS mechanisms improve the convergence performance to different degrees. From the standpoint of the unknown system's sparsity, with the variety of system SRs, the convergence MSDs of all candidate algorithms are increased. Compared with other VSS mechanisms, the proposed algorithm is feasible to the unknown system with different sparsity. Some insights can be obtained from the Fig. 5 and Fig. 6. The proposed algorithm has a low steady-state MSD with a slightly fast convergence rate. This is because each step-size optimization increment takes into account the gradient from the steady-state MSD to the step-size, and the corresponding MSD is minimized when the optimal value of the step-size is obtained for each iteration. It is important to note that the step-size should

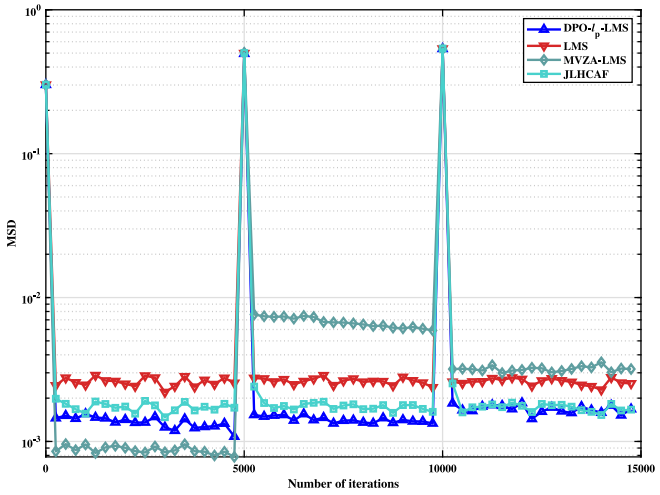

Fig. 5. MSD curves of DPO-l_p-LMS, LMS, MVZA-LMS, and JLHCAF with various SRs.

be constrained by the Eq. (20) [39], which can be ensured by a smaller value of α ,β.

Overall, the results indicate that the proposed algorithm achieves excellent performances in terms of modeling accuracy and system tracking ability. Thus, it is feasible for time-varying UWA communication applications [31,40].

5. Experiment and analysis

Based on a real-world sea trial, the proposed algorithm DPO-l_p-LMS and the other algorithms (i.e., l_1-LMS, l_0-LMS, LMS, JLHCAF, and MVZA-LMS) are adopted in UWA direct-adaptation turbo equalization (DA-TEQ) for the purpose of performance comparison and evaluation.

Table 3
Parameters in the Second experiment between LMS, JLHCAF, MVZA-LMS, and DPO-l_p-LMS

Algorithms	Parameters
LMS	$\mu = 2e-2$
DPO-l_p-LMS	$\mu_{ini} = 2e-2, \kappa = 2e-4, \alpha = 1e-6, \beta = 1e-5$
JLHCAF	$\mu = 2e-2, \lambda = 7.5e-1, \rho = 1e-7, a = 2e-1$
MVZA-LMS	$\mu = 2e-2, \rho = 1e-3, a = 1$

5.1. DA-TEQ with the DPO-l_p-LMS algorithm

A single-carrier single-input-multiple-output (SIMO) UWA communication system is considered. Fig. 7 shows the detailed system structure. In the transmitter site, the information bit sequence **a** of length n is encoded by a forward error code (FEC) encoder, and the coded bits **b** are interleaved **c** and mapped to symbols **s** and transmitted. Propagation through the UWA channel with L length, the baseband signal received at time instant k can be expressed as follow (the ideal state is assumed in the receiver site) [41]:

$$y_k = \sum_{l=0}^{L-1} h_l s_{k-l} + w_k, \tag{22}$$

where the s_{k-l} is the transmitted symbol at the time $k-1$, the h_l is the lth coefficient of UWA baseband channel impulse responses between the transmitter and the receiver, and the w_k is the additive noise. On the receiver side, the DA-TEQ is adopted for symbol recovery.

As shown in the Fig. 7, the equalizer compute the extrinsic likelihood ratio (LLR) of the interleaved bit $\lambda_e\{c_n\}$ from the equalized symbol $\hat{x}_n$. The extrinsic LLRs $\lambda_e\{\mathbf{c}\}$ be regarded as the prior information passing into the decoder after de-interleave. Afterward, the decoder output the extrinsic information of the coded bits $\lambda_e\{\mathbf{b}\}$. The prior information will be passed to the equalizer in the next

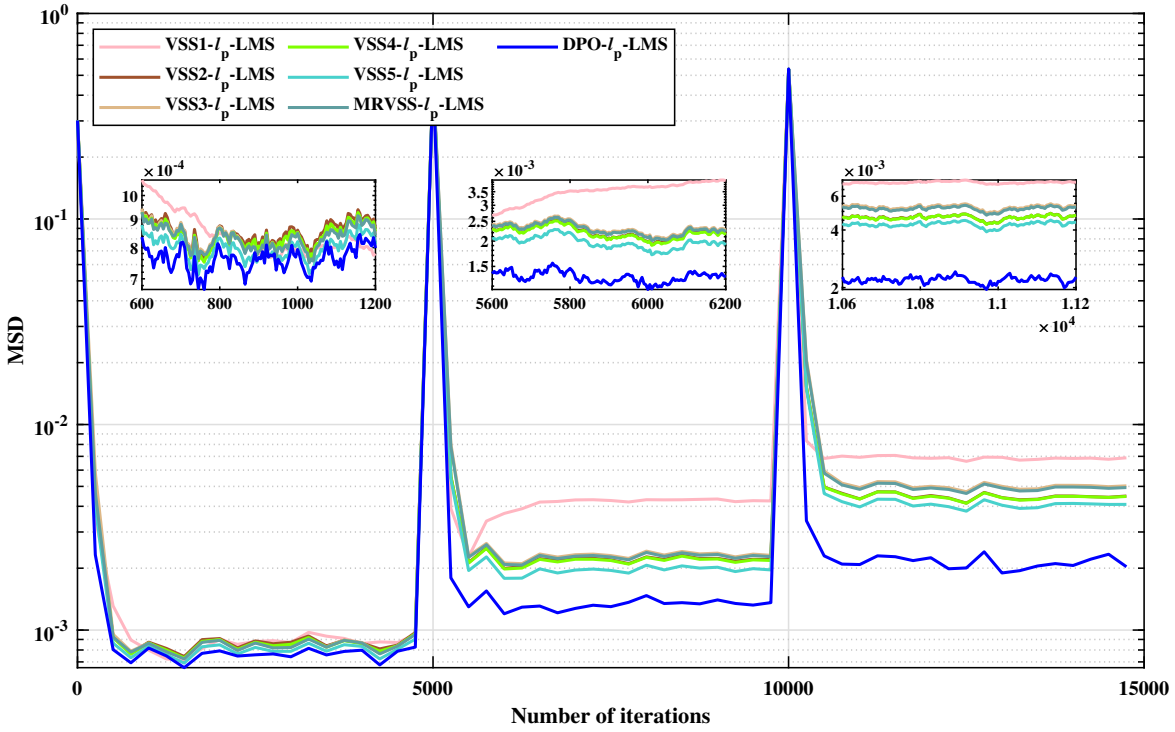

Fig. 6. MSD curves of l_p-LMS aided by different VSS mechanisms with various SRs.

Table 4
Parameters set up in the Second experiment

Algorithm Name	Parameter
VSS1-l_p-LMS	$a = 0.1, b = 1, \beta = 0.98, \kappa = 0.00015, p = 0.85, T = 1$
VSS2-l_p-LMS	$\alpha = 1000, \beta = 0.02, m = 3, \kappa = 0.0003, p = 0.85, T = 1$
VSS3-l_p-LMS	$\alpha = 100, \beta = 0.009, \gamma = 1, \kappa = 0.0003, p = 0.85, T = 1$
VSS4-l_p-LMS	$a = 100, b = 2, c = 0.01, m = 2, \kappa = 0.0003, p = 0.85, T = 1$
VSS5-l_p-LMS	$\alpha = 0.97, \gamma = 0.0005, \mu_{ini} = 0, \mu_{min} = 0.01, \mu_{max} = 0.017, \kappa = 0.0003, p = 0.85, T = 1$
MRVSS-l_p-LMS	$\mu_{ini} = 0.03, \alpha = 0.9, \gamma = 0.003$, a = 0.9, b = 0.99999, $\kappa = 0.0003, p = 0.85, T = 1$
DPO-l_p-LMS	$\mu_{ini} = 0.015, \alpha = 0.000002, \beta = 0.0001, \mathbf{g} = 0, \kappa = 0.0003, p = 0.85, T = 1$

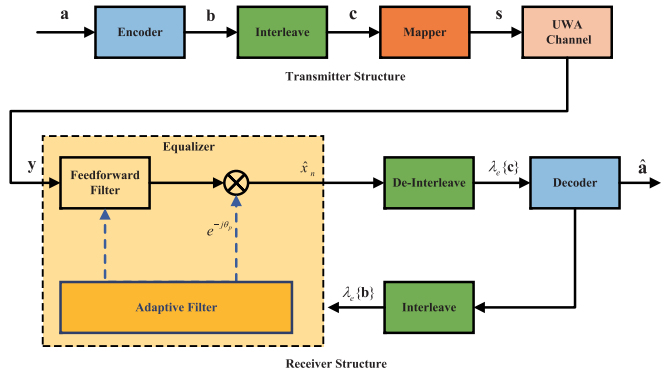

Fig. 7. The structure of UWA system.

iteration after interleaving. Meanwhile, the decoder also outputs the hard-decision information bits $\hat{\mathbf{a}}$. With multiple exchanges of information between the equalizer and decoder, the reliability of the hard-decision information bits will be improved. The detailed approaches for computing the LLRs can be referenced from these papers [42,43].

For the equalized symbol $\hat{x}_n$, it can be computed as:

$$\hat{x}_n = \mathbf{f}_n^H \mathbf{y}_n e^{-j\hat{\theta}_p(n)}, \tag{23}$$

where the $\mathbf{f}_n$ represents the feedforward filter coefficients. The $\mathbf{y}_n$ is the receive vector, and the $\tilde{\mathbf{d}}_n$ decision symbol vectors. The $\hat{\theta}_p$ is the estimation phase generated by phase locked loop (PLL) [44] for phase correction.

The updated of the $\mathbf{f}_n$ under the minization mean square error (MMSE) criterion can be expressed as [44]:

$$\mathbf{f}_n = \mathbf{f}_{n-1} - \mu_f e_n^* \mathbf{y}_n e^{-j\hat{\theta}_p(n)}, \tag{24}$$

where the e_n is the decision error between the training symbol and the estimated symbol, and the μ_f is the update step-size for the adaptive filter algorithm.

5.2. Results analysis

The field experiment was conducted in Wuyuan Bay, Xiamen, China, with the map of which presented in Fig. 8. A SIMO UWA communication system was deployed as shown in Fig. 9. Two transducers were mounted on the Tx site and Rx site, respectively. The Tx transducer was placed about 4 m below the sea surface, while the Rx transducers were placed approximately 3 m and 4 m below, respectively. The water depth in Wuyuan Bay was about 8 m, with a measured sound velocity profile as shown in Fig. 9. The horizontal communication range between the Tx and Rx was approximately 800 m.

The carrier frequency was 13–18 kHz, the symbol rate was 1.2 k symbols/s, and the sampling frequency of the receiver was 96 kSps. The packet format of the transmit signal is presented in Fig. 10,

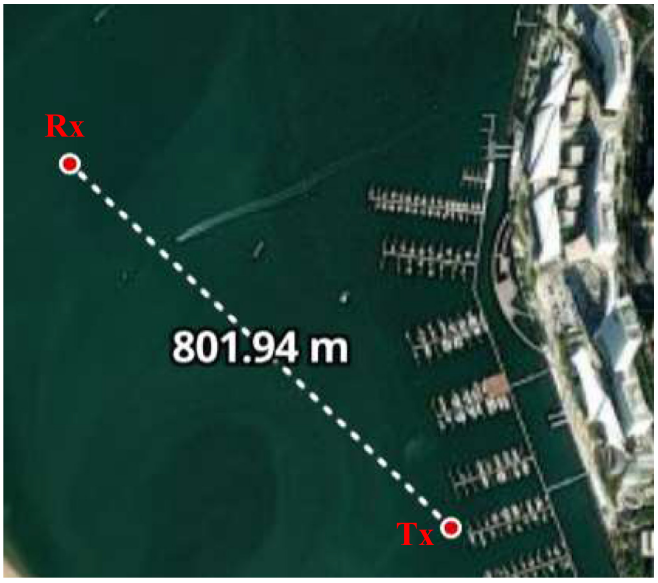

Fig. 8. The UWA communication sea trial in Wuyuan Bay. (Tx, Rx represents the transmitter site, receiver site respectively.)

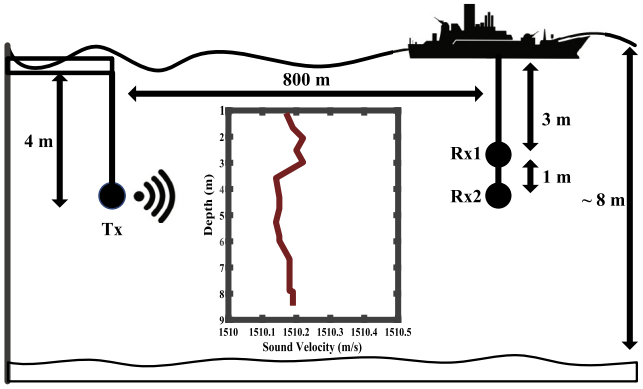

Fig. 9. The deployment of the sea experiment in Wuyuan Bay.

Fig. 10. The packet format of the transmit signal in the sea experiment.

consisting of a linear frequency modulation (LFM) preamble, training sequences, and data frame. In the data sequences, the information bits were encoded, interleaved, and modulated into 768 binary

phase shift keying (BPSK) symbols. The information bits were encoded using the turbo product code (TPC) with rate-1/2, and the Chase algorithm was adopted for decoding. During the experiment, long-term noise data were also collected during the experiment to test the performance of DA-TEQ.

For DA-TEQ, the channel estimation is not required. However, the adaptive channel estimation algorithm based on LMS was employed to illustrate the channel structure clearly. The estimated UWA channels were presented in Fig. 11 (denoted as Ch1, Ch2, respectively). For the channel of Ch1, the UWA channel exhibits a dynamic sparse structure with uncertain sparsity, and the first arrival block with the strongest energy appears at around 4 ms, determined by both the direct and the first surface bouncing sound rays. Similar to channel of Ch1, the channel of Ch2 also exhibits a sparse structure with varying sparsity, and the channel only has the most vital energy at around 5 ms, corresponding to the direct propagation path. Through alone the Geo-time direction, the sparsity of the UWA channel changes constantly and presents a significant uncertain sparsity with the time evolution. The sparsity of channel of Ch1 and Ch2 has changed, possibly influenced by the marine environment after 0.25 s. In terms of the channel structure of Ch1 and Ch2, the channel of Ch2 is more sparse than Ch1 with slowly time-varying sparsity. That is means that the data recovery for Ch2 will be easy than Ch1.

Following the principle of DA-TEQ, the LMS, l_1-LMS, l_0-LMS and the DPO-l_p-LMS were employed to update the equalizer coefficients, respectively. The length of the feedforward filter is set as 4. The specific parameters of the equalizer are given in Table 5, where for LMS types of DA-TEQ, the μ_f is the step-size, and for DPO-l_p-LMS types of DA-TEQ, the $\mu_{f_{ini}}$ is the initial step-size, the κ is the parameters of the sparse regular term, the α, β is the parameters for adjusting the step-size. The bit error rate (BER) is a metric index of the DA-TEQ in the condition of various SNRs illustrated in Fig. 12.

Some phenomenons can be observed from Fig. 12. As the number of iterations increases, the BER decreases gradually. After nine iterations, the DPO-l_p-LMS type DA-TEQ achieves zero BER in the condition of -2 dB measured noise under Ch1, and -3 dB measured noise under Ch2. In Ch1, the DA-TEQ driven by proposed algorithm performs better than LMS, l_1-LMS, l_0-LMS, JLHCAF, and MVZA-LMS driven when the iteration has not yet started. This is because other algorithms (LMS, l_1-LMS, l_0-LMS, JLHCAF, and MVZA-LMS type DA-TEQ) presuppose a constant sparse pattern,

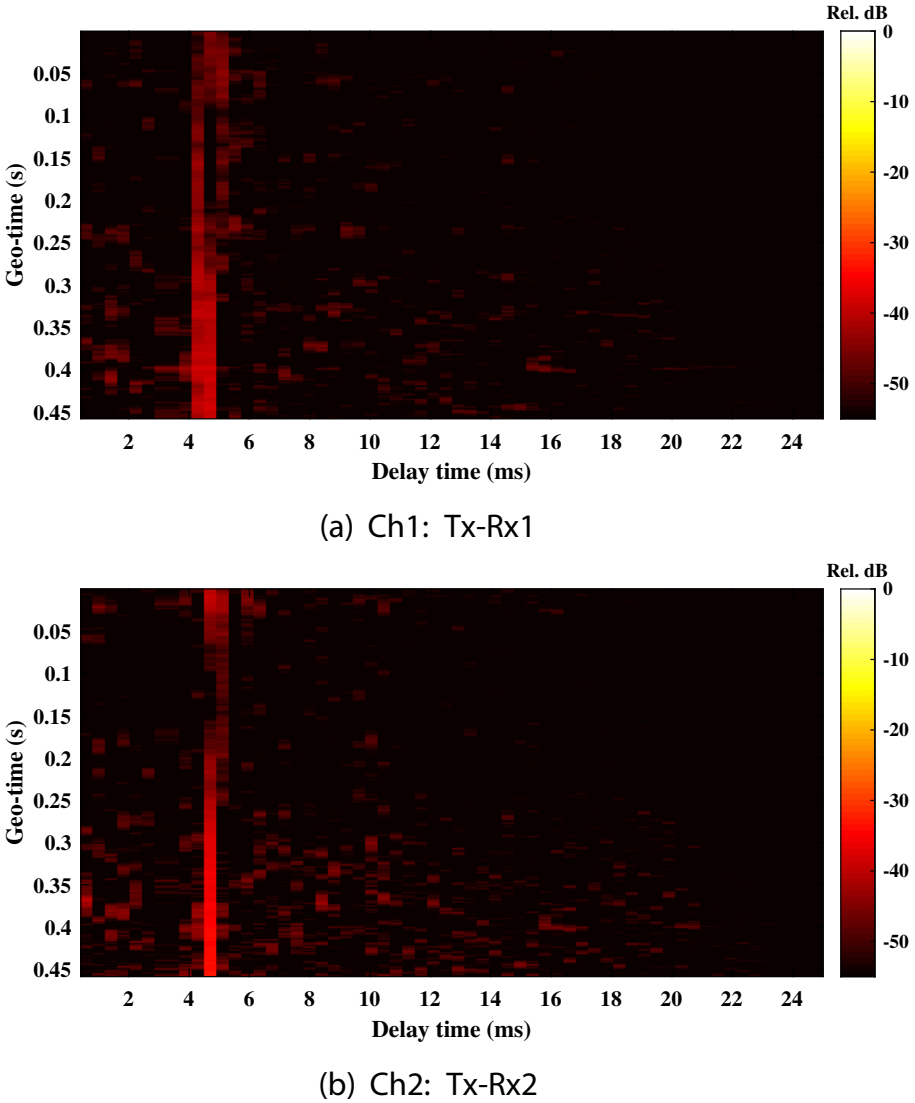

Fig. 11. Channel impulse responses estimated via LMS algorithm.

Table 5
Parameters set up of LMS, DPO-l_p-LMS, l_1-LMS, and l_0-LMS

DA-TEQ Type	Parameters	
	Ch1	Ch2
LMS	$\mu_f = 3e-1$	$\mu_f = 3e-2$
DPO-l_p-LMS	$\mu_{f_{ini}} = 4.5e-1, \kappa = 4e-4, \alpha = 1e-6$	$\mu_{f_{ini}} = 3e-2, \kappa = 5e-4, \alpha = 2e-7$
	$\beta = 1e-5, p = 0.85$	$\beta = 1e-5, p = 0.85$
l_1-LMS	$\mu_f = 3e-1, \kappa = 4e-4$	$\mu_f = 3e-2, \kappa = 4e-4$
l_0-LMS	$\mu_f = 3e-1, \kappa = 4e-4$	$\mu_f = 3e-2, \kappa = 4e-4$
JLHCAF	$\mu_f = 3e-1, \lambda = 7.5e-1, \rho = 1e-7, a = 2e-1$	$\mu_f = 3e-2, \lambda = 8.5e-1, \rho = 1e-7, a = 2e-1$
MVZA-LMS	$\mu_f = 3e-1, \rho = 1e-3, a = 1$	$\mu_f = 3e-2, \rho = 1e-3, a = 0.9$

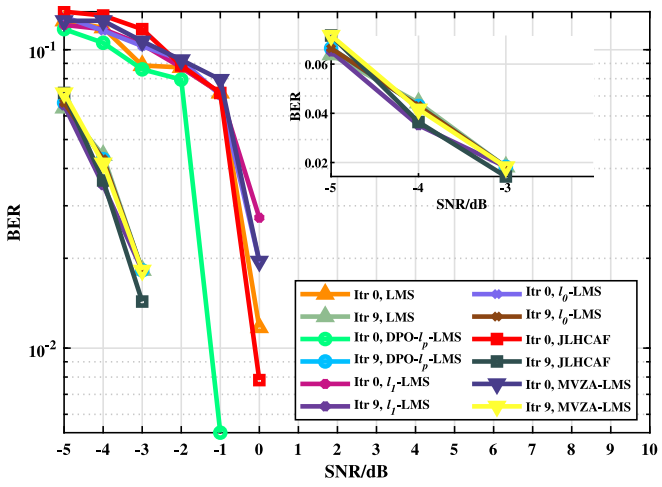

(a) Ch1: Tx-Rx1

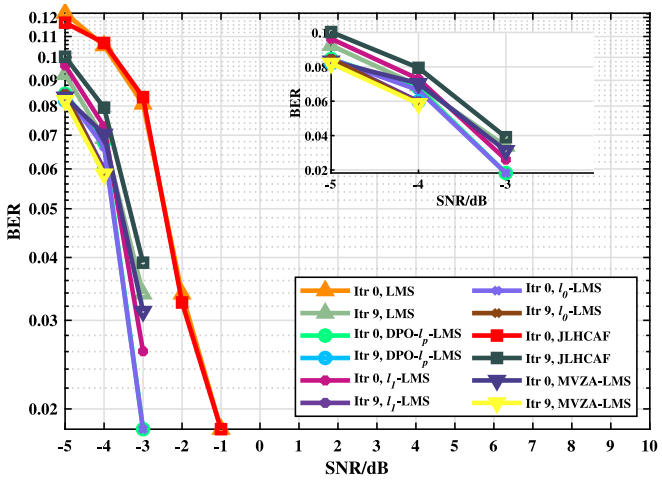

(b) Ch2: Tx-Rx2

Fig. 12. The performance of DA-TEQ in Ch1, and Ch2.

and there is a mismatch for the channel of Ch1 with uncertain sparsity, resulting in recovery performance impact.

Meanwhile, for other algorithms, the step-size of each iteration is not optimal and the best feedforward filter taps cannot be obtained quickly and accurately. As the iterative equalization proceeds, it can be seen that all algorithms eventually achieve zero BER in the −2 dB measured noise. In Ch2, the performance of all the algorithms is significantly improved before starting the iteration equalization, which is due to the simpler structure of Ch2. Specifically, the DA-TEQ performance driven by DPO-l_p-LMS, l_1-LMS, l_0-LMS, and MVZA-LMS enables zero BER in the −2 dB measured noise without iteration equalization, while this performance bound requires nine DA-TEQ iterative equalizations driven by the LMS and JLHCAF to be achieved. The performances improved of l_1-LMS, l_0-LMS, and MVZA-LMS type DA-TEQ should be contributed on the constant sparsity in Ch2. This phenomenon is consistent with the conclusion obtained by numerical simulation, i.e., the proposed algorithm performs better in more sparse systems than the LMS, JLHCAF.

6. Conclusion

A dual parameters optimization l_p-LMS (DPO-l_p-LMS) algorithm is proposed for temporal-spatial varying sparse UWA channel. By converting the complicated dual parameter optimization problem into a parallel gradient descent iteration, the proposed algorithm is capable of alleviating the problem of low convergence speed and high steady-state error. Finally, numerical simulation and field UWA communication experiment in shallow water indicate that the proposed DPO-l_p-LMS yields better performance in UWA communication when compared with other variants of l_p-LMS algorithms, at the presence of uncertain sparsity.

Data availability

The authors are unable or have chosen not to specify which data has been used.

Declaration of Competing Interest

The authors declare that they have no known competing financial interests or personal relationships that could have appeared to influence the work reported in this paper.

Acknowledgement

This work was supported in part by the National Key Research and Development Program of China (No. 2018YFE0110000), in part by the National Natural Science Foundation of China (Nos. 11274259, 11574258), in part by the R&D institution construction project supported by Shenzhen Virtual University Park (YFJGJS1.0), in part by the Science and Technology Commission Foundation of Shanghai (21DZ1205500), in part by the National Natural Science Foundation of China (No. 62171369).

References

[1] Haykin Simon. Adaptive Filter Theory. Pearson Education; 2013.
[2] Jin Jian, Qing Qu, Yuantao Gu. Robust zero-point attraction least mean square algorithm on near sparse system identification. IET Signal Proc May 2013;7 (3):210–8.

[3] Jin Jian, Yuantao Gu, Mei Shunliang. Adaptive algorithm for sparse system identification: Zero-attracting LMS. J Tsinghua Univ (Sci Technol) 2010;50(10):1656–9.
[4] Yuantao Gu, Jin Jian, Mei Shunliang. L0-Norm Constraint LMS Algorithm for Sparse System Identification. IEEE Signal Process Lett September 2009;16(9):774–7.
[5] Jin Jian, Yuantao Gu, Mei Shunliang. A Stochastic Gradient Approach on Compressive Sensing Signal Reconstruction Based on Adaptive Filtering Framework. IEEE J Selected Top Signal Process April 2010;4(2):409–20.
[6] Wu FY, Tong F. Non-Uniform Norm Constraint LMS Algorithm for Sparse System Identification. IEEE Commun Lett February 2013;17(2):385–8.
[7] Shi Kun, Shi Peng. Convergence analysis of sparse LMS algorithms with l1-norm penalty based on white input signal. Signal Process December 2010;90(12):3289–93.
[8] Guolong Su, Jin Jian, Yuantao Gu, Wang Jian. Performance Analysis of l0-Norm Constraint Least Mean Square Algorithm. IEEE Trans Signal Process May 2012;60(5):2223–35.
[9] Kumar Krishna, Pandey Rajlaxmi, Karthik MLNS, Subhra Bhattacharjee Sankha, George Nithin V. Robust and sparsity-aware adaptive filters: A Review. Signal Process December 2021;189:108276.
[10] Sankha Subhra Bhattacharjee, Dwaipayan Ray, Nithin V. George, Adaptive Modified Versoria Zero Attraction Least Mean Square Algorithms. IEEE Trans Circuits Syst., 67(12):5, 2020.
[11] Kumar Krishna, Bhattacharjee Sankha Subhra, George Nithin V. Joint Logarithmic Hyperbolic Cosine Robust Sparse Adaptive Algorithms. IEEE Trans Circuits Syst II Express Briefs January 2021;68(1):526–30.
[12] Duttweiler DL. Proportionate normalized least-mean-squares adaptation in echo cancelers. IEEE Trans Speech Audio Process Sept./2000.;8(5):508–18.
[13] Paleologu Constantin, Benesty Jacob, Ciochina Silviu. An improved proportionate NLMS algorithm based on the l0 norm. In: 2010 IEEE International Conference on Acoustics, Speech and Signal Processing, ICASSP 2010. Dallas, TX: IEEE; March 2010. p. 309–12.
[14] Taheri Omid, Vorobyov Sergiy A. Sparse channel estimation with lp-norm and reweighted l1-norm penalized least mean squares. In: ICASSP 2011–2011 IEEE International Conference on Acoustics, Speech and Signal Processing (ICASSP). IEEE.: Prague, Czech Republic; May 2011. p. 2864–7.
[15] Feiyun Wu, Zhou Yuehai, Tong Feng. Estimation algorithm for sparse channels with gradient guided p-norm like constraints. J Commun 2014;35(7):172–7.
[16] Wu FY, Tong F. Gradient optimization p-norm-like constraint LMS algorithm for sparse system estimation. Signal Process April 2013;93(4):967–71.
[17] Kwong RH, Johnston EW. A variable step size LMS algorithm. IEEE Trans Signal Process July 1992;40(7):1633–42.
[18] Aboulnasr Tyseer, Mayyas K. A Robust Variable Step-Size LMS-Type Algorithm: Analysis and Simulations. IEEE Trans Signal Process 1997;45(3):9.
[19] Luo Xiaodong, Jia Zhenghong, Wang Qiang. A New Variable Step Size LMS Adaptive Filtering Algorithm. Acta Electron Sinica 2006;6:1123–6.
[20] Xiuqun Du, Feng Xian, Wei Du. A Variable Step Size LMS Algorithm Applied to Adaptive Noise Cancellation. Mech Sci Technol Aerosp Eng 2010;29(12):1732–4.
[21] Wang Pingbo, Ma Kai, Cai Wu. Segmented variable-step-size LMS algorithm based on normal distribution curve. J National Univ Defense Technol 2020;42(5):16–22.
[22] Biao Wang, Li Hanqiong, Gao Shijie, Zhang Mingliang, Chen Xu. A Variable Step Size Least Mean p-Power Adaptive Filtering Algorithm. J Electron Inform Technol 2022;44(02):661–7.
[23] Shengkui Zhao, Zhilong Man, Suiyang Khoo. A fast variable step-size LMS algorithm with system identification. In: 2007 2nd IEEE Conference on Industrial Electronics and Applications. Harbin, China: IEEE; 2007. p. 2340–5.
[24] Aliyu Muhammad Lawan, Alkassim Mujahid Ado, Salman Mohammad Shukri. A p-norm variable step-size LMS algorithm for sparse system identification. SIViP October 2015;9(7):1559–65.
[25] Geng Xueyi, Zielinski Adam. An eigenpath underwater acoustic communication channel model. 'Challenges of Our Changing Global Environment'. Conference Proceedings. OCEANS '95 MTS/IEEE, volume 2. San Diego, CA, USA: IEEE; 1995. p. 1189–96.
[26] Zou Zheguang, Badiey Mohsen. Effects of Wind Speed on Shallow-Water Broadband Acoustic Transmission. IEEE J Oceanic Eng October 2018;43(4):1187–99.
[27] Xingbin Tu, Xiaomei Xu, Song Aijun. Statistical analysis and hybrid modeling of high-frequency underwater acoustic channels affected by wind-driven surface waves. J Acoust Soc Am May 2022;151(5):3266–79.
[28] Pelekanakis Konstantinos, Chitre Mandar. Robust Equalization of Mobile Underwater Acoustic Channels. IEEE J Oceanic Eng October 2015;40(4):775–84.
[29] Xia Menglu, Rouseff Daniel, Ritcey James A, Zou Xiang, Polprasert Chantri, Wen Xu. Underwater Acoustic Communication in a Highly Refractive Environment Using SC–FDE. IEEE J Oceanic Eng July 2014;39(3):491–9.
[30] Zhou Yue-hai, Jiang Wei-hua, Tong F, Zhang Gang-qiang. Exploiting joint sparsity for underwater acoustic MIMO communications. Appl Acoust January 2017;116:357–63.
[31] Jiang Weihua, Tong Feng, Zhu Zhengliang. Exploiting rapidly time-varying sparsity for underwater acoustic communication. IEEE Trans Veh Technol 2022:1–15.
[32] Jiang Weihua, Tong Feng, Zheng Siyuan, Cao Xiuling. Estimation of Underwater Acoustic Channel With Hybrid Sparsity via Static-Dynamic Discriminative Compressed Sensing. IEEE Sens J December 2020;20(23):14548–58.
[33] Qin Zhen, Tao Jun, Fengzhong Qu, Qiao Yongjie. Adaptive equalization based on dynamic compressive sensing for single-carrier multiple-input multiple-output underwater acoustic communications. J Acoust Soc Am May 2022;151(5):2877–84.
[34] Tao Jun, Yanbo Wu, Han Xiao, Pelekanakis Konstantinos. Sparse Direct Adaptive Equalization for Single-Carrier MIMO Underwater Acoustic Communications. IEEE J Oceanic Eng October 2020;45(4):1622–31.
[35] Bragard P, Jourdain G. A fast self-optimized LMS algorithm for non-stationary identification: Application to underwater equalization. In: International Conference on Acoustics, Speech, and Signal Processing. Albuquerque, NM, USA: IEEE; 1990. p. 1425–8.
[36] Mathews VJ, Xie Z. A stochastic gradient adaptive filter with gradient adaptive step size. IEEE Trans Signal Process June 1993;41(6):2075–87.
[37] Douglas SC, Pan Weimin. Exact expectation analysis of the LMS adaptive filter. IEEE Trans Signal Process Dec./1995.;43(12):2863–71.
[38] Mandar Chitre. The Acoustics Toolbox is distributed under the GNU Public License.http://oalib.hlsresearch.com/AcousticsToolbox/.
[39] Farhang-Boroujeny Behrouz. Adaptive filters: theory and applications. John Wiley & Sons; 2013.
[40] Jiang Weihua, Tong Feng. Exploiting sparsity for underwater acoustic sensor network under time-varying channels. IEEE Internet Things J 2022;9(4):2859–69.
[41] Proakis John G, Salehi Masoud. Digital Communications. 5th ed edition,. Boston: McGraw-Hill; 2008.
[42] Wang Zhenduo, Zhe Xie Wu. Zhou, and Hongtao Zhang. Mean Doppler Compensation for SIMO Turbo Equalization in Underwater Acoustic Communications. In: 2019 IEEE International Conference on Signal Processing, Communications and Computing (ICSPCC). Dalian, China: IEEE; September 2019. p. 1–6.
[43] Xi Junyi, Yan Shefeng, Lijun Xu, Hou Chaohuan. Sparsity-Aware Adaptive Turbo Equalization for Underwater Acoustic Communications in the Mariana Trench. IEEE J Oceanic Eng January 2021;46(1):338–51.
[44] Stojanovic M, Catipovic JA, Proakis JG. Phase-coherent digital communications for underwater acoustic channels. IEEE J Oceanic Eng Jan./1994.;19(1):100–11.